Submicrosecond Electron Transfer to Monolayer-Bound Redox Species on Gold Electrodes at Large Overpotentials

David B. Robinson and Christopher E. D. Chidsey*

Department of Chemistry, Stanford University, Stanford, California 94305-5080

Received: May 28, 2002; In Final Form: July 23, 2002

Chronoamperometry with microscopic line electrodes was used to measure rates of electron transfer between gold electrodes and monolayer-bound ferrocenes for a variety of short chain lengths (5 to 13 methylenes) and at overpotentials exceeding 1 V. The rates vary from 10^2 s^{-1} to 3×10^7 s^{-1} and show an exponential chain-length dependence with a decay constant of 1.1 per CH_2 over the measured overpotential range. The potential dependence of the rates for these short chain lengths follows the predictions of the Marcus−Levich model of interfacial electron transfer. The reorganization energy is near the value of 0.8 eV previously reported for similar systems. A thorough understanding of this system is likely to be an important foundation in the broader understanding of electron transport through organic materials, which is facilitated by access to fast rates over wide potential ranges.

I. Introduction

It has been recognized for many decades that long-distance electron transfer through molecules is a phenomenon exploited by biological systems to provide a wide variety of functionality, including the transduction of light into stored chemical energy by photosynthesis and the subsequent use of that energy by respiration. This phenomenon may also offer a valuable range of properties for use in the development of microelectronic devices. Many investigators are working to develop new electronic devices that incorporate organic molecular layers as electron-transport media and that take advantage of the properties and versatility of molecules.[1−9] Whereas some clever approaches and exciting properties have been reported, the technology for assembly of single molecules and other nanoscale components into robust and reproducible two- and three-terminal electronic devices is still in its infancy. Thorough and quantitative studies of electron transfer in single-molecule device structures remain extremely challenging, and the range of observables available to characterize them is very limited. The well-established methods of electrochemistry applied to an electrode−molecular monolayer−electrolyte interface offer the ability to answer many thermodynamic, kinetic, and structural questions relevant to the construction of electronic devices that are difficult or impossible to address in single-molecule device structures.

Electrochemical systems using redox-active molecules tethered to organic monolayer-coated electrodes have been shown to be among the most well-defined and versatile ways to study the mechanisms of molecular electron transfer and of tunneling through organic materials.[10−20] The study of electron transfer at electrode surfaces allows the reaction free energy to be tuned by adjusting the electrode potential. Self-assembled organic monolayers can provide the structure that establishes a tunneling barrier between the electrode and redox molecules. This can decrease electron-transfer rates to time scales that are easy to measure. The components of organic monolayers can be tailored with atomic precision, and the layers can be characterized by a variety of independent techniques.[21] The use of tethered species removes the diffusion of redox molecules to the electrode as a necessary step in an electrochemical measurement, which can otherwise obscure the measurement of electron-transfer rates. By diluting redox-active molecules with analogous, inactive monolayer components, the environment of the redox molecules can be controlled such that the redox-active species behave nearly independently and nearly uniformly.

Such systems have been used to demonstrate that electron-tunneling rates through trans oligomethylene chains decay with natural logarithmic constants of about 1 per methylene unit over a range of chain lengths.[12] They have also been used to show that the Marcus theory of electron transfer, using Levich's application to metal electrodes, provides a simple yet reasonably accurate explanation of the mechanism of electron transfer at these interfaces.[11,12,22,23] Other work using nontethered redox molecules has helped confirm these conclusions.[24−26] Use of conjugated linker molecules between the redox molecule and electrode dramatically reduces the distance dependence of the electron-transfer rate.[15,27−29]

Electron-transfer rate constants can be directly measured as a function of potential using chronoamperometry, a method in which the interfacial potential is stepped from one potential to another and the current to the electrode is measured. This method can be used to map the rate constant as a function of reaction free energy over a wide range of free energies. Unfortunately, the rapid and large changes of the interfacial potential required to measure the rate of electron transfer can in some cases be difficult to accomplish. To produce the required potential step, it is necessary to charge the interfacial capacitance more rapidly than the rate of electron transfer. The charging time is determined by the cell resistance and interfacial capacitance and by the response time of feedback circuits used to control the interfacial potential. The method can also be limited by the quality of the monolayer because large back-

* Corresponding author. E-mail: chidsey@stanford.edu.

10.1021/jp026195+ CCC: $22.00
Published on Web 09/24/2002

ground currents and irreversible changes in the monolayer structure at large overpotentials can obscure the electron-transfer process. For these reasons, measurements of fast electron-transfer rates and of rates under conditions of large changes in free energy have often been impossible by chronoamperometry.

These limitations can be overcome by using microelectrodes, which allow faster rates to be measured.[30] As the electrode area decreases, solution resistance increases, but interfacial capacitance decreases more rapidly, so smaller electrodes result in faster cell-charging times. Also, many background processes are less pronounced at faster time scales, making it easier to observe fast electron transfer at high overpotentials.

Microelectrodes allow for several other improvements that can increase the maximum measurable rates. The small amounts of charge drawn by microscopic electrodes cause negligible polarization of a macroscopic reference electrode, so a three-electrode control loop is not necessary. Forster and Faulkner have used chronoamperometry to measure the distance and potential dependence of electron-transfer rates through a redox-active monolayer on a platinum microelectrode.[31] Studies by Creager et al. have used AC voltammetry with monolayer-coated gold microelectrodes.[15]

It is also possible to avoid partially or completely the use of real-time feedback loops to compensate for measurement or cell resistance. If the experimental time scale is fast enough to ensure reproducible behavior, an iterative feedback procedure can be used in which a correction calculated from the previous iteration of the experiment is applied, as demonstrated by Wipf.[32] A combination of iterative and real-time feedback allows a wide range of time scales to be accessed.

The ferrocene−alkanethiol−gold monolayer system is an especially valuable target for study because alkanethiol monolayers have been thoroughly characterized through the work of many investigators and because related monolayers have been a primary structural component of most molecular electronic devices reported recently. Application of microelectrode techniques is challenging for the ferrocene−alkanethiol−gold system because it is difficult to fabricate well-sealed gold microelectrodes that expose only a microscopic electrode area and because permeation currents tend to be high for monolayers on unoriented, polycrystalline gold wires, especially at large overpotentials.[33,34] Experiments on macroscopic monolayer systems usually use surfaces that are primarily composed of (111) crystallite faces, such as those made by the evaporation of gold.[35] We have found that the use of planar, microscopic lines of evaporated gold yields electrochemical behavior comparable to macroscopic evaporated electrodes while allowing access to much faster time scales.

This paper demonstrates the application of these techniques and presents chronoamperometric results for ferrocene−alkanethiol−gold systems that are 3 orders of magnitude faster than those of previous reports. It shows that the systems behave consistently over a range of chain lengths and a range of interfacial potentials of about ±1 V. This helps demonstrate the general applicability of the semiempirical Marcus−Levich model. It also sets a basis for comparison with monolayers that contain conjugated components, which transfer electrons more rapidly and over longer distances than alkanethiols and are being used in multiple-terminal molecular electronic devices.

II. Theoretical Background

A. Electrochemical Theory. Simple theoretical descriptions can be applied when redox species tethered dilutely to the solution side of a monolayer behave as an ensemble of identical and independent redox sites with weak electronic coupling of each site to the electrode and the remainder of the monolayer behaves as a linear capacitor.[36] The equilibrium redox charge state $q_{\mathrm{redox}}^{\mathrm{eq}}$ of such a system should obey the Nernst equation

$$q_{\mathrm{redox}}^{\mathrm{eq}}(E) = \frac{eN}{1 + \exp\left(-\frac{e(E - E^{0'})}{k_{\mathrm{B}}T}\right)} \quad (1)$$

where e is the magnitude of the charge of an electron, N is the number of redox sites, E is the interfacial potential, $E^{0'}$ is the formal potential of the redox species, k_{B} is the Boltzmann constant, and T is the temperature. The sum of this charge and the double-layer charge q_{dl} (assumed proportional to the potential) fully describes the total equilibrium charge state of the system.

The electron-transfer rate for a redox species at an electrode was derived from the kinetic theory of Marcus by Levich and others.[37−40] The theory assumes that the electron can tunnel between the electrode and redox site when the structure of the site and its environment has caused the free energy and molecular arrangement of the initial and final states to be the same, a condition that generally requires thermal activation. The tunneling process is described by the Landau−Zener model for transitions between weakly coupled diabatic states with time-dependent energy levels.[41] The energy levels are determined by assuming parabolic reactant and product free-energy surfaces as described by Marcus, parametrized by the standard free energy of reaction and a reorganization energy, λ, that is the same for reactants and products. The value of λ for a monolayer-tethered redox site in contact with an electrolyte solution has been predicted to be very close to the expected value for the same redox species dissolved in the electrolyte for the monolayer thicknesses used here.[42,43] The electrode is assumed to be composed of a distribution of one-electron states, populated according to the Fermi−Dirac distribution. We approximate the Fermi−Dirac distribution as a convolution of a step function and a Gaussian-shaped thermal-broadening term, chosen to best approximate the exact values predicted for the true Fermi−Dirac distribution.[44] These assumptions result in the following form for the reduction and oxidation rate constants:

$$k_{\substack{\mathrm{red}\\ \mathrm{ox}}}(E) = \frac{\pi\rho|H_{12}|^2}{\hbar}\,\mathrm{erfc}\left(\frac{\lambda \pm e(E - E^0)}{\sqrt{4k_{\mathrm{B}}T(\lambda + 1.75k_{\mathrm{B}}T)}}\right) \quad (2)$$

where ρ is the local density of states in the electrode, $\hbar$ is Planck's constant, H_{12} is the electronic coupling matrix element, $\mathrm{erfc}(x)$ is the complementary error function, and the upper and lower subscripts on the rate constant correspond to the upper and lower signs in the argument of the erfc function, respectively. For simplicity, we have assumed that $\rho|H_{12}|^2$ is not dependent on the interfacial potential, an assumption that has been supported by previous experiments on nearly identical systems.[11] This assumption provides a conceptual separation of tunneling effects from the potential dependence. To the extent that it is valid, this assumption allows these phenomena to be studied independently.

Three differential equations can be derived that, with eqs 1 and 2, completely describe the charge state of the system as a function of a time-dependent applied potential E_{app}, including the effect of uncompensated cell resistance R. The first is simply

the net first-order rate law

$$\frac{dq_{redox}}{dt} = k_{et}(q_{redox}^{eq}(E) - q_{redox}) \quad (3)$$

where $k_{et} \equiv k_{red} + k_{ox}$ is the electron-transfer relaxation rate constant. The second is Ohm's law applied to the potential drop across the cell resistance, where q is the total charge:

$$\frac{dq}{dt} = \frac{E_{app} - E}{R} \quad (4)$$

The third is the definition of capacitance applied to the double layer, where C_{dl} is the double-layer capacitance and the double-layer charge is the difference between the total and redox charges:

$$\frac{dE}{dt} = \frac{1}{C_{dl}}\left(\frac{dq}{dt} - \frac{dq_{redox}}{dt}\right) \quad (5)$$

These equations can be used to simulate numerically the current response to any applied potential, so the results of any voltammetric or chronoamperometric experiments can be used to test whether the assumptions made here apply to the ferrocene−monolayer−gold system.

B. Linear Dynamics. An intuitive model is available to aid understanding of the chronoamperometric response. If the electrochemical rate constants are assumed to be independent of potential and the equilibrium charge is assumed to be linearly dependent on potential (rather than the actual sigmoidal form of eq 1), then the equations can be solved analytically, with a simple limiting form:

$$k_{cell} \approx k_{et} \qquad \text{when} \qquad k_{et} \ll \frac{k_{dl}}{1+\gamma}$$

where k_{dl} is the reciprocal of RC_{dl} and γ is the ratio of redox charge to double-layer charge passed in the experiment. This ratio can be adjusted by changing the monolayer composition or the initial potential of the experiment and is usually about 1 in our measurements. The double-layer charging rate k_{dl} is thus on the order of the maximum measurable rate for a given electrode.

C. Microelectrode Parameters. Microelectrodes allow the measurement of substantially faster electron-transfer rates for tethered systems than for those measured at macroscopic electrodes because they have a larger value of k_{dl}. This can be understood by examining the geometric dependence of the cell parameters.[45] For a hemicylindrical electrode, the solution resistance is approximately

$$R \cong \frac{\rho}{\pi L}\ln\left(\frac{2L}{W}\right) \quad (6)$$

where ρ is the resistivity of the solution and W and L are the width and length of the electrode. This assumes that the sizes of the cell and reference electrode are comparable to L. Because the electrodes used here are actually planar, ion transport to the electrode is further restricted, and the resistance is somewhat higher. Finite difference calculations suggest that the resistance is higher by a factor of about 2. There is an additional contribution to the resistance due to the electrode wire itself. The double-layer capacitance is approximately

$$C_{dl} \cong \frac{\epsilon\epsilon_0 LW}{d} \quad (7)$$

where ϵ is the dielectric constant of the monolayer, ϵ_0 is the permittivity of free space, and d is the monolayer thickness. The approximate double-layer charging rate is then

$$k_{dl} \cong \left[\frac{\rho\epsilon\epsilon_0}{d}W\ln\left(\frac{2L}{W}\right)\right]^{-1} \quad (8)$$

which increases approximately linearly as the line width decreases.

D. Applied and Interfacial Potential. The goal of chronoamperometry is to measure the electron-transfer relaxation rate constant at a series of interfacial potentials. This is most simply achieved by applying a potential step to the cell, but if enough current flows to make the potential drop across the cell resistance significant, then the interfacial potential will not be constant, confounding the measurement. This problem can be solved by feeding a signal derived from the measured current back to change the applied potential continuously in real time, but this can introduce speed and stability limitations. An alternate technique is iterative control, where the correction is calculated after the experiment and the experiment is repeated.[32,46,47] The version implemented here is similar to that used by Wipf but is optimized for a capacitive system that primarily experiences exponential transients as a result of a changing potential.

The applied potential necessary to produce a step in the capacitor potential of a series RC circuit is a step function plus an infinitely sharp exponential spike, where the charge passed by the additional component is equal to the required capacitive charge. The control signal used by Wipf's method is proportional to the circuit's current transient. This signal can be adjusted to approximate the optimal control signal more closely by using a control element known as a lead compensator, which effectively deconvolutes a slow exponential and replaces it with a fast one. The correction y for a given iteration can be computed from the difference x between the measured and desired values from the previous iteration, given as a time-ordered array of sampled points indexed by n:

$$y_n = y_{n-1}\exp(-\alpha k_s \Delta t) + G\alpha(x_n - x_{n-1}\exp(-k_s\Delta t)) \quad (9)$$

where G is a gain parameter, α is the ratio of the time constants of the fast and slow exponentials, k_s is the decay rate of the slow exponential, and Δt is the sampling interval.[48] We have set the slow time constant to the observed decay time (see below), α to 3, and G to 1 in our experiments.

III. Experimental Section

A. Electrode Fabrication. Planar gold microelectrodes consisted of 2-mm square contact pads, 100-μm × 2.5-mm leads, and 4-μm × 1.25-mm line electrodes (Figure 1). Contact mask fabrication and photoresist patterning were performed at the Stanford Nanofabrication Facility. The sample substrate was a Pyrex 7740 glass wafer (Bullen Ultrasonics). Wafers were cleaned in a 2-propanol/potassium hydroxide bath, rinsed, baked at 150° C for 5 min, and cooled. A 300-nm layer of liftoff resist (Shipley LOL2000, 1500 rpm for 60 s, baked 5 min at 170 °C) and a 1.1-μm layer of photoresist (Shipley 3612, 5000 rpm for 30 s, baked 60 s at 90 °C) were applied to each wafer. The wafers were exposed under the contact mask to 16-mW/cm^2 UV for 0.8 s. Exposed wafers were developed in a commercial

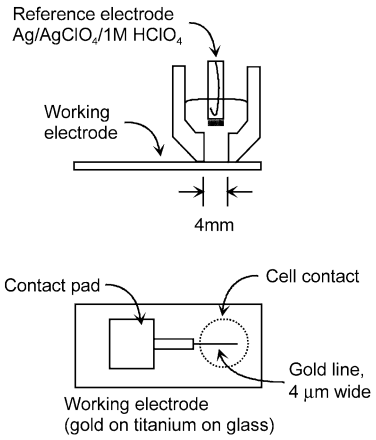

Figure 1. Schematic drawing of cell and microelectrode geometry.

tetramethylammonium hydroxide-based developer (Shipley LDD26W) for 60 s with agitation, rinsed thoroughly, blown dry, and baked for 60 s at 110 °C. Titanium (10 to 20 nm) and gold (100 to 200 nm) were evaporated onto the wafers at approximately 0.2 nm/s in an electron-beam evaporator. Photoresist was lifted off by sonicating wafers in *N*-methyl-2-pyrrolidone (Shipley 1165) for 1 h, rinsing with water, and blowing dry. Wafers were then baked at 100 °C for 60 s and coated as above with photoresist as a protective layer. Wafers were cut with a wafer saw to create individual samples 14 mm wide and 3 cm long. Each sample contained a 8-mm × 12-mm gold area in addition to microelectrodes to allow for characterization by macroscopic electrochemistry. Other macroelectrodes were prepared by a similar evaporation onto bare silicon wafers. The resistance of the line electrodes was measured to be 100 Ω.

B. Monolayer Preparation. Immediately before use, individual resist-coated microelectrodes were sonicated for 5 min in *N*-methyl-2-pyrrolidone and rinsed thoroughly. Microelectrodes or macroelectrodes were cleaned in a mixture of 9 volumes of 30 wt % aqueous hydrogen peroxide and 1 volume of sulfuric acid for 10 s, rinsed, soaked for 1 min in 5 wt % hydrochloric acid, rinsed, blown dry, rinsed with ethanol, and blown dry. (**Caution:** mixtures of hydrogen peroxide and sulfuric acid can react explosively with organic materials.) Electrodes were placed in vials of freshly prepared solutions of 100 μM alkanethiol and 5 to 50 μM of the corresponding ferrocenecarbonyl alkanethiol in ethanol. Electrodes were soaked overnight, rinsed with ethanol, blown dry, and used immediately.

C. Electrochemical Measurements. Measurements were performed with a cell consisting of a cylindrically bored Teflon cone (4-mm inner diameter) pressed against the sample. The exposed microelectrode length, *L*, was 1−2 mm. The cone was filled with 1 M aqueous perchloric acid. A platinum counter electrode and a glass frit-isolated silver/dilute silver perchlorate/1 M aqueous perchloric acid reference electrode were suspended in the cell. The reference electrode resistance was measured to be 150 Ω by cyclic voltammetry in a three-electrode cell at low speeds and in a two-electrode cell on a 100-ns time scale. An Analogue Devices AD 825 operational amplifier with a switchable feedback resistor was used as a current-to-voltage converter. The response time of this converter was 30 ns when the feedback resistance was 267 Ω, the value used for fast chronoamperograms. Potential programs were generated by a Wavetek 395 function generator. Current responses were recorded using a Tektronix TDS 520 digital oscilloscope. Measurements were performed at room temperature (20−22 °C).

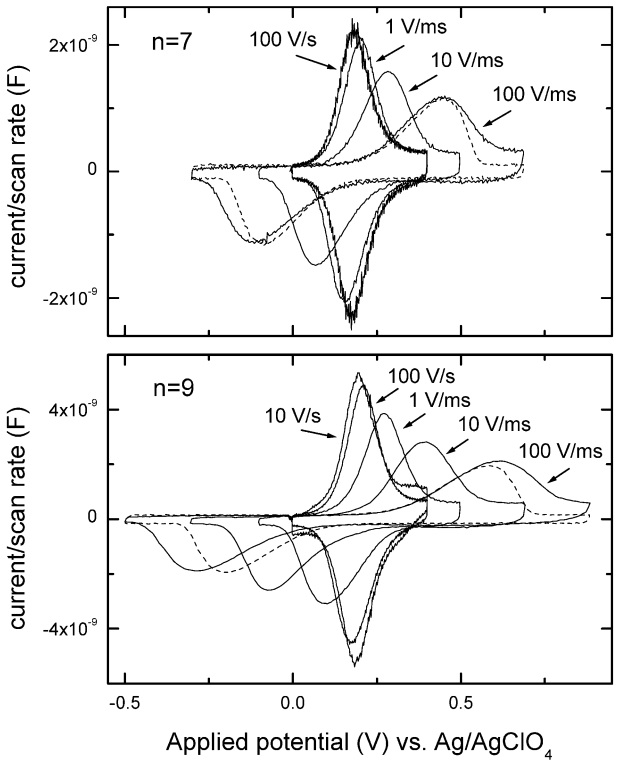

Figure 2. Cyclic voltammograms of electrodes with monolayers formed from $FcCO_2(CH_2)_nSH$ and $H(CH_2)_nSH$, $n = 7$ and 9, at various scan rates (—) and a simulated voltammogram (− − −) at the highest scan rate for each chain length.

IV. Results

A. Cyclic Voltammetry. To gain an understanding of the thermodynamics of the redox species as well as some initial kinetic information, monolayer-coated electrodes were characterized by cyclic voltammetry. Figure 2 shows voltammograms for several scan rates and chain lengths. Voltammograms at the slowest scan rates for each chain length approach the ideal shapes for a tethered monolayer system at equilibrium, with no peak splitting and with peak widths of 98 to 105 mV. Peak widths approaching 90 mV at room temperature are a signature of an ensemble of uniform and independent redox molecules.[36] As the scan rate increases, the redox charge lags behind the equilibrium value. With increasing overpotential, the rate constant increases, so the charge can pass more readily. The longer chain length shows a greater peak splitting at a given scan rate, indicating slower rate constants. The formal potentials of all systems were 170−190 mV versus the reference electrode (measured to be 720 mV vs NHE). It should be noted that the background current on the positive side of the redox peak is consistently several times greater than that on the negative side, indicating permeation of electrolyte ions into the monolayer. We have found this to be a reversible behavior that is independent of the presence of tethered ferrocene.[33]

Equations 1−5 can be used to simulate the voltammograms at all scan rates. In Figure 2, simulations of the voltammogram at the highest scan rate for each chain length are shown. The charge parameters were determined from the low-speed voltammograms, and kinetic parameters were determined from the chronoamperometric data discussed below. Good qualitative agreement is obtained, although the experimental peaks are 20 to 60% broader than expected. We defer further discussion until after presenting the chronoamperometric results.

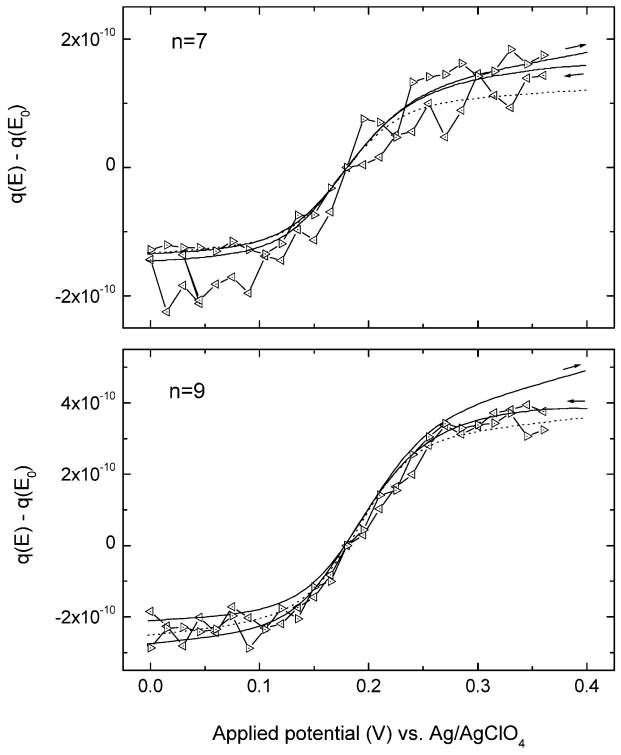

Figure 3. Plots of charge versus applied potential for electrodes with monolayers formed from $FcCO_2(CH_2)_nSH$ and $H(CH_2)_nSH$, $n = 7$ and 9, measured by cyclic voltammetry at 100 mV/ms (—) and chronoamperometry (lines with markers), along with a simulation of the integrated equilibrium charge using the theory discussed in section II (·····). For left-pointing markers, the final step potential was −60 mV; for right-pointing markers, 420 mV.

B. Coulometry. To ensure that the charge passed in high-speed chronoamperometric experiments is the same as that passed in low-speed voltammetry experiments, a series of applied potential steps were made from many potentials near the formal potential to a potential relatively far from the formal potential. The integrated charge passed in these experiments was compared to the time integrals of the slow cyclic voltammograms. Figure 3 shows that the amount of charge passed is approximately the same in all experiments and follows the predicted shape of the equilibrium charge (eq 1) summed with the charge from a potential-independent double-layer capacitance.

C. Microelectrode Parameters. According to the predictions described above, a 4-μm × 2-mm line electrode in 1 M perchloric acid ($\rho = 5$ Ω cm) with a 1-nm dielectric film ($\epsilon = 2.2$) should have a solution resistance of about 100 Ω, a double-layer capacitance of 160 pF, and a double-layer charging rate of 1.6×10^8 s^{-1}. Measured capacitance values agreed with this. The total cell resistance was measured to be 450 Ω. Subtracting the measured reference-electrode resistance of about 150 Ω and the measured line-electrode resistance of about 100 Ω leaves a solution resistance of about 200 Ω, twice the expected value. Capacitances were measured by cyclic voltammetry, and resistances were measured from peak currents of chronoamperograms. A resistance of 400 Ω was used in the compensation algorithm; full or excess compensation of cell resistance can introduce stability problems. Including a redox charge comparable to the amount of double-layer charge passed ($\alpha = 1$), the fastest measurable rate is expected to be roughly 3×10^7 s^{-1}, about the same as the measured response time of the current-to-voltage converter.

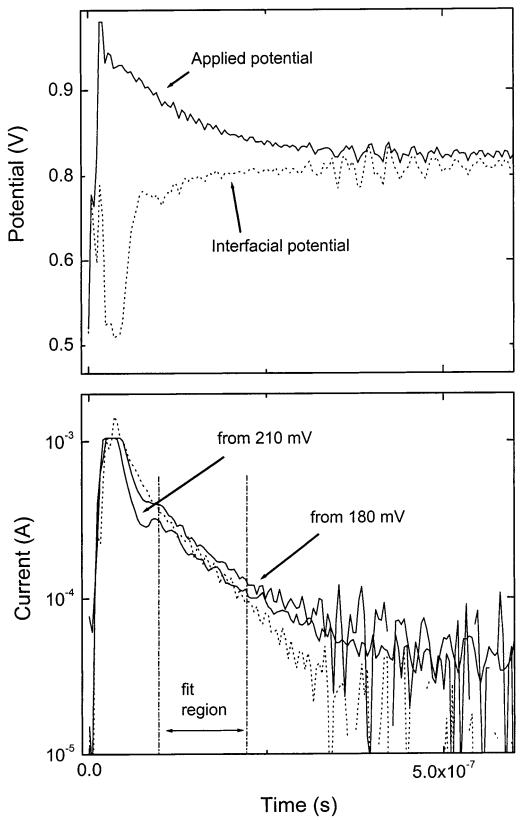

Figure 4. Typical chronoamperograms for monolayers formed from $FcCO_2(CH_2)_{10}SH$ and $H(CH_2)_{10}SH$, showing both potential and current curves. The applied potential (—) had been corrected iteratively to compensate for 400 Ω of cell resistance. The expected interfacial potential assuming the full measured resistance of 450 Ω is shown (- - -). The current plot shows the effect of an incremental change in redox charge as well as a simulated curve (- - -). Simulation parameters include fits to the low-speed voltammogram, the measured rate constant at $E^{0\prime}$, and an assumed reorganization energy of 0.8 eV.

D. Chronoamperometry. Figure 4 shows representative examples of the fastest chronoamperograms from these experiments. The upper plot shows the continuously varying applied potential used for the chronoamperogram in the lower plot starting at 180 mV as well as the calculated interfacial potential based on the measured cell resistance of 450 Ω.

The lower plot shows that there is an initial double-layer charging spike, a redox decay, and a finite background current. An incremental change in the redox charge, effected by changing the initial potential, helps identify the region of the curve where redox current dominates. There is an offset to the curve in this region but no change in slope. The logarithmic slope was determined in this region, typically over a range of 1 to 2 time constants. The absolute value of this slope was taken to be k_{et} at the mean interfacial potential measured over the same time interval. Initial potentials were chosen to provide enough redox charge for such a measurement, but not more, to prevent large potential drops across the cell resistance.

A comparison of the upper and lower plots shows that the interfacial potential varies by no more than a few tens of millivolts in the region of measurement. However, if the measured cell resistance is inaccurate, then the error in the interfacial potential may be larger. Simulations have shown that a cell resistance error range of ±100 Ω would result in a 50% uncertainty in the measured rate for rates of the magnitude shown in Figure 4.[49] As rates decrease from the values around 10^7 s^{-1} characteristic of this Figure, both the corrections and

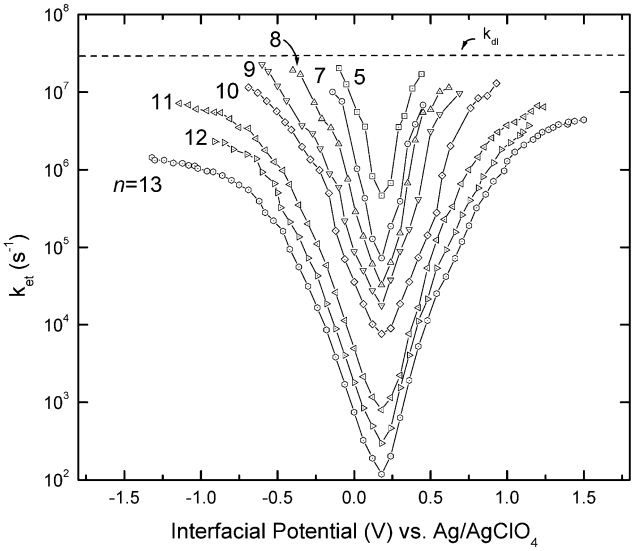

Figure 5. Interfacial potential dependence of the rate constants observed on microelectrodes for monolayers formed from $FcCO_2(CH_2)_n$-SH and $H(CH_2)_nSH$, $n = 5$ and 7−13.

the uncertainty become less significant. These corrections for cell resistance are significant when rates exceed 10^6 s^{-1} and when the rate constant changes rapidly with increasing potential.

E. Potential Dependence. The k_{et} values extracted from the microelectrode chronoamperometry experiments are shown as a function of overpotential in Figure 5. The values reported are averages over measurements from 1 to 3 starting potentials and 1 to 3 samples. Variations among those measurements were generally less than a factor of 3 and thus less than the gaps between adjacent curves. The curves increase exponentially at moderate positive and negative overpotentials but gradually saturate at both very positive and very negative overpotentials. The Figure shows that an approximately exponential chain-length dependence is present over nearly the entire range of chain lengths and potentials and over more than 5 orders of magnitude in rate.

F. Chain-Length Dependence. Plots of electron-transfer rate constants at several overpotentials for chain lengths of $n = 5-13$ are shown in Figure 6. The natural logarithmic decay constant β, $(-d(\ln k_{et})/dn)$, is 1.1 per CH_2, closely matching the value predicted and observed by others.[12,16,24−26] The parallel nature of the curves in Figure 5 indicates that the value of β is nearly constant as a function of overpotential. The data are comparable to the potentiometric indirect laser-induced temperature-jump (ILIT) measurements made at moderate overpotentials by Smalley et al. for the shorter-chain ferrocenes.[16] The ILIT data are shown for comparison in the Figure.

G. Simulations of Potential Dependence. Figure 7 shows comparisons of data for two chain lengths from Figure 5 to the predictions of the Marcus−Levich theory using the measured values of k_{et} at $E = E^{0'}$ and various reorganization energies. Both curves approach the expected symmetric Butler−Volmer slopes of ±120 mV/decade at moderate overpotentials. The Butler−Volmer model assumes linearly varying free-energy surfaces. The $n = 12$ curve gradually saturates at higher overpotentials, as predicted by the Marcus−Levich theory, which assumes parabolic free-energy surfaces.

A simulation of the chronoamperogram in Figure 4 that stepped from 180 to 780 mV is shown as a dashed line in that Figure. The simulation used the value of k_{et} at $E = E^{0'}$ from Figure 5 and $\lambda = 0.8$ eV, a value representative of previous predictions and measurements and that roughly describes the n = 12 curve in Figure 7.[16,42] The measured k_{et} value for the experiment was 8.9×10^6 s^{-1}. The rate extracted from the simulation was 1.1×10^7 s^{-1}, demonstrating agreement comparable to that shown in Figure 7.

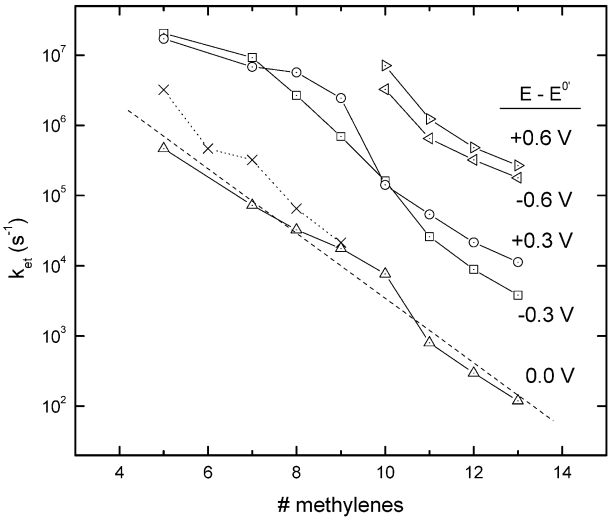

Figure 6. Chain-length dependence of the rate constant at several overpotentials (open symbols). The decay constant β is 1.1 per methylene; a fit to the zero-overpotential curve using this decay constant is shown (− − −). The potentiometric ILIT data from Smalley et al.[16] are included for comparison (×).

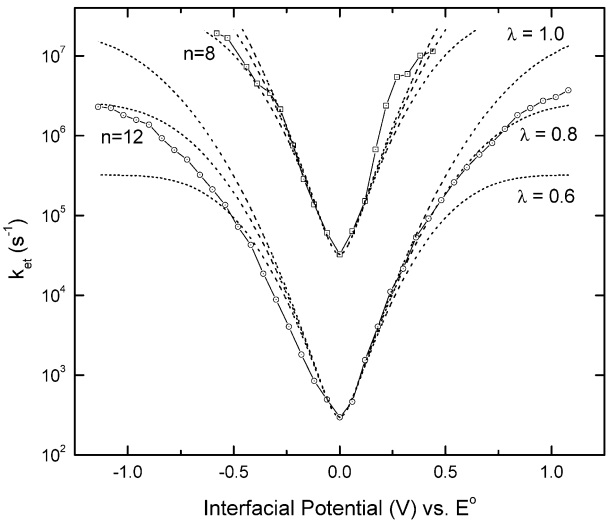

Figure 7. Comparison of measured rate data for $n = 8$ and 12 to the Marcus−Levich model (eqs 2 and 3) using the measured rate constant at $E^{0'}$ and reorganization energies of 0.6, 0.8, and 1.0 eV.

Predictions of the Marcus−Levich theory are also shown for the fastest cyclic voltammograms in Figure 2 (dashed lines). Parameters for the simulation were determined in the same way as for the simulation in Figure 4. The simulations predict less lag of the reduction peaks than that observed experimentally, indicating that the predicted rate constants are faster than the actual values. A similar discrepancy can also be observed in Figure 7 at negative overpotentials. In addition, the simulated peaks are somewhat narrower than those observed experimentally.[50]

The deviations from the predictions shown in these Figures could be caused by factors not included in the theory, such as static or dynamic irregularities in the structure of the monolayer or electrostatic interaction of neighboring redox sites that may influence the electron-transfer rate at high overpotentials for shorter lengths.[36] Although tethering redox sites to a monolayer

restricts the ability of the sites to be transported to defective regions of a monolayer, it is reasonable to expect that tethered sites will still be influenced by nonuniformities in their local environment. To reduce variations in the measured data or deviations from theoretical predictions, it is probably necessary to use even more compact, uniform monolayers than those we have so far been able to obtain with *n*-alkanethiols. Monolayer quality might be further improved by the use of chains with larger cross-sectional area, such as regularly branched alkanes or perfluorinated alkanes.[21,51] However, such chains with an appropriate redox group on one end and a thiol on the other have yet to be synthesized.

V. Conclusions

We have shown that chronoamperometry of ferrocene-terminated monolayers on gold can be extended to rates on the order of 10^7 s^{-1}—much faster than the previously reported chronoamperometric rates of 10^4 s^{-1} for this system—using methodological improvements associated with the use of microelectrodes. It is possible that this approach could be extended to higher rates by decreasing the electrode area further and by using iterative correction for the measurement resistance as well as the cell resistance instead of real-time feedback. The presence of measurement capacitance and other parasitic circuit elements such as line inductance would complicate the measurement of rates much more than an order of magnitude faster than those reported here. It may be possible to overcome some of these limitations through the use of a miniaturized buffer circuit on or very near the sample.

Analysis of the ferrocene−alkanethiol−gold system by chronoamperometry and cyclic voltammetry has shown correspondence with simple theoretical predictions and consistent behavior over a wide range of chain lengths. The dependence of the electron-transfer rate constant on chain length is exponential over the entire range of chain lengths and overpotentials measured, with an essentially constant logarithmic slope. This offers validity to the useful conceptual separation of the electron-transfer mechanism into independent electron-tunneling and structural reorganization processes. At high overpotentials, the saturation of the electron-transfer rates predicted by the Marcus−Levich model was clearly observed for chain lengths 9 through 13; for shorter chain lengths, the phenomenon is expected to occur at rates too fast for us to measure. At fast rates and high overpotentials, it appears that there are several other factors that influence the measurement in addition to those included in the simple theory, including rearrangement or permeation of the monolayer.

A thorough understanding of the behavior of such redox-active monolayer−gold interfaces is likely to facilitate development and understanding of devices where two or three electrodes are in intimate contact with a small number of molecules, which are likely to involve delocalization of electrons by tunneling and localization of electrons by reorganization processes. It would also help build an understanding of molecules that facilitate long-distance electron transfer. Fast chronoamperometry can provide a direct view of a wide range of information that is valuable toward accomplishing these goals.

Acknowledgment. D.B.R. acknowledges financial support from the National Science Foundation, Atofina Inc., and the John Stauffer Foundation. C.E.D.C. acknowledges key discussions with S.B. Sachs and S.W. Feldberg. Ferrocenecarbonyl alkanethiols were synthesized by T.M. Putvinski.

References and Notes

(1) Mann, B.; Kuhn, H. *J. Appl. Phys.* **1971**, *42*, 4398.
(2) Polymeropoulos, E. E.; Sagiv, J. *J. Chem. Phys.* **1978**, *69*, 1836.
(3) Schon, J. H.; Meng, H.; Bao, Z. *Nature (London)* **2001**, *413*, 713.
(4) Holmlin, R. E.; Haag, R.; Chabinyc, M. L.; Ismagilov, R. F.; Cohen, A. E.; Terfort, A.; Rampi, M. A.; Whitesides, G. M. *J. Am. Chem. Soc.* **2001**, *123*, 5075.
(5) Collier, C. P.; Jeppesen, J. O.; Luo, Y.; Perkins, J.; Wong, E. W.; Heath, J. R.; Stoddart, J. F. *J. Am. Chem. Soc.* **2001**, *123*, 12632.
(6) Slowinski, K.; Fong, H. K. Y.; Majda, M. *J. Am. Chem. Soc.* **1999**, *121*, 7257.
(7) Slowinski, K.; Majda, M. *J. Electroanal. Chem.* **2000**, *491*, 139.
(8) Chen, J.; Reed, M. A.; Rawlett, A. M.; Tour, J. M. *Science (Washington, D.C.)* **1999**, *286*, 1550.
(9) Zhou, C.; Deshpande, M. R.; Reed, M. A.; Jones, L.; Tour, J. M. *Appl. Phys. Lett.* **1997**, *71*, 611.
(10) Li, T. T. T.; Weaver, M. J. *J. Am. Chem. Soc.* **1984**, *106*, 6107.
(11) Chidsey, C. E. D. *Science (Washington, D.C.)* **1991**, *251*, 919 with the correction: Chidsey, C. E. D. *Science (Washington, D.C.)* **1991**, *252*, 631.
(12) Finklea, H. O.; Hanshew, D. D. *J. Am. Chem. Soc.* **1992**, *114*, 3173.
(13) Finklea, H. O.; Hanshew, D. D. *J. Electroanal. Chem.* **1993**, *347*, 327.
(14) Finklea, H. O.; Ravenscroft, M. S.; Snider, D. A. *Langmuir* **1993**, *9*, 223.
(15) Creager, S.; Yu, C. J.; Bamdad, C.; O'Connor, S.; MacLean, T.; Lam, E.; Chong, Y.; Olsen, G. T.; Luo, J. Y.; Gozin, M.; Kayyem, J. F. *J. Am. Chem. Soc.* **1999**, *121*, 1059.
(16) Smalley, J. F.; Feldberg, S. W.; Chidsey, C. E. D.; Linford, M. R.; Newton, M. D.; Liu, Y. P. *J. Phys. Chem.* **1995**, *99*, 13141.
(17) Sachs, S. B.; Dudek, S. P.; Hsung, R. P.; Sita, L. R.; Smalley, J. F.; Newton, M. D.; Feldberg, S. W.; Chidsey, C. E. D. *J. Am. Chem. Soc.* **1997**, *119*, 10563.
(18) Sikes, H. D.; Smalley, J. F.; Dudek, S. P.; Cook, A. R.; Newton, M. D.; Chidsey, C. E. D.; Feldberg, S. W. *Science (Washington, D.C.)* **2001**, *291*, 1519.
(19) Weber, K.; Hockett, L.; Creager, S. *J. Phys. Chem. B* **1997**, *101*, 8286.
(20) Sumner, J. J.; Weber, K. S.; Hockett, L. A.; Creager, S. E. *J. Phys. Chem. B* **2000**, *104*, 7449.
(21) Chidsey, C. E. D.; Loiacono, D. N. *Langmuir* **1990**, *6*, 682.
(22) Forster, R. J.; Faulkner, L. R. *J. Am. Chem. Soc.* **1994**, *116*, 5444.
(23) Smalley, J. F.; Feldberg, S. W.; Chidsey, C. E. D.; Linford, M. R.; Newton, M. D.; Liu, Y. P. *J. Phys. Chem.* **1995**, *99*, 13141.
(24) Becka, A. M.; Miller, C. J. *J. Phys. Chem.* **1992**, *96*, 2657.
(25) Xu, J.; Li, H. L.; Zhang, Y. *J. Phys. Chem.* **1993**, *97*, 11497.
(26) Slowinski, K.; Chamberlain, R. V.; Miller, C. J.; Majda, M. *J. Am. Chem. Soc.* **1997**, *119*, 11910.
(27) Sachs, S. B.; Dudek, S. P.; Hsung, R. P.; Sita, L. R.; Smalley, J. F.; Newton, M. D.; Feldberg, S. W.; Chidsey, C. E. D. *J. Am. Chem. Soc.* **1997**, *119*, 10563.
(28) Forster, R. J.; Figgemeier, E.; Loughman, P.; Lees, A.; Hjelm, J.; Vos, J. G. *Langmuir* **2000**, *16*, 7871.
(29) Sikes, H. D.; Smalley, J. F.; Dudek, S. P.; Cook, A. R.; Newton, M. D.; Chidsey, C. E. D.; Feldberg, S. W. *Science (Washington, D.C.)* **2001**, *291*, 1519.
(30) Forster, R. J. *Chem. Soc. Rev.* **1994**, *23*, 289.
(31) Forster, R. J.; Faulkner, L. R. *J. Am. Chem. Soc.* **1994**, *116*, 5453.
(32) Wipf, D. O. *Anal. Chem.* **1996**, *68*, 1871.
(33) Creager, S. E.; Hockett, L. A.; Rowe, G. K. *Langmuir* **1992**, *8*, 854.
(34) Hockett, L. A.; Creager, S. E. *Langmuir* **1995**, *11*, 2318.
(35) Hou, Z. Z.; Dante, S.; Abbott, N. L.; Stroeve, P. *Langmuir* **1999**, *15*, 3011.
(36) Bard, A. J.; Faulkner, L. R. *Electrochemical Methods*, 2nd ed.; John Wiley & Sons: New York, 2001.
(37) Marcus, R. A. *J. Chem. Phys.* **1955**, *24*, 966.
(38) Marcus, R. A. *J. Chem. Phys.* **1965**, *43*, 679.
(39) Gerischer, H. *Z. Phys. Chem. N. F.* **1960**, *26*, 325.
(40) Levich, V. G. In *Advances in Electrochemistry and Electrochemical Engineering*; Delahay, P., Tobias, C. W., Eds.; Wiley-Interscience: New York, 1966; Vol. 4, p 249.
(41) Zener, C. *Proc. R. Soc. London, Ser. A* **1932**, *137*, 696.
(42) Liu, Y. P.; Newton, M. D. *J. Phys. Chem.* **1994**, *98*, 7162.
(43) Liu, Y. P.; Newton, M. D. *J. Phys. Chem.* **1995**, *99*, 12382.
(44) This approximation was tested for a range of λ/k_BT values from 0.01 to 100 and results in errors of less than 4% in the sum $k_{red} + k_{ox}$ over

this range. The broadening parameter 1.75 was chosen to minimize error at $E = E^{0'}$ when $\lambda = 0.8$ eV. For individual rate constants, it is best to use this equation for negative free energies of reaction and to use that value and the Nernst equation to compute the corresponding rate for positive free energies of reaction, as discussed in Nahir, T. M. *J. Electroanal. Chem.* **2002**, *518*, 47.

(45) Wightman, R. M.; Wipf, D. O. *Electroanalytical Chemistry*; Bard, A. J., Ed.; Marcel Dekker: New York, 1989; Vol. 15, p 267.

(46) Chen, Y. *Iterative Learning Control*; Springer: New York, 1999.

(47) Moore, K. L.; Dahleh, M.; Bhattacharyya, S. P. *J. Robotic Systems* **1992**, *9*, 563.

(48) Franklin, G. F.; Powell, J. D.; Emami-Naeini, A. *Feedback Control of Dynamic Systems*; Addison-Wesley: New York, 1994.

(49) The resistance of the line electrode is expected to produce a variation of $\pm 25\ \Omega$ along the length of the electrode exposed to the electrolyte solution.

(50) Cell resistance does affect the shape of the high-speed cyclic voltammograms, but the uncertainty in the observed cell resistance is not sufficient to explain the discrepancy between the experiments and simulations.

(51) BraachMaksvytis, V.; Raguse, B. *J. Am. Chem. Soc.* **2000**, *122*, 9544.